PHYSICAL REVIEW C **75**, 054304 (2007)

Nuclear hyperdeformation and the Jacobi shape transition

N. Schunck,[1,2] J. Dudek,[3] and B. Herskind[2]
[1]*Departamento de Fisica Teorica, Universidad Autonoma de Madrid, 28049 Cantoblanco, Madrid, Spain*
[2]*The Niels Bohr Institute, University of Copenhagen, DK-2100 Copenhagen, Denmark*
[3]*Institut de Recherches Subatomiques IN$_2$P$_3$-CNRS/Université Louis Pasteur, F-67037 Strasbourg Cedex 2, France*
(Received 6 October 2006; published 3 May 2007)

The possibility that atomic nuclei possess stable, extremely elongated (hyperdeformed) shapes at very high angular momentum is investigated in the light of the most recent experimental results. The crucial role of the Jacobi shape transitions for the population of hyperdeformed states is discussed and emphasized. State-of-the-art mean-field calculations including the most recent parametrization of the liquid-drop energy together with thermal effects and minimization algorithms allowing the spanning of a large deformation space predict the existence of a region of hyperdeformed nuclei in the mass $A \sim 120$–130: Te, Cs, Xe, I, and Ba isotopes. In agreement with predictions presented in reviews by J. Dudek, K. Pomorski, N. Schunck, and N. Dubray [Eur. Phys. J. A **20**, 15 (2003)] and J. Dudek, N. Schunck, and N. Dubray [Acta Phys Pol. B **36**, 975 (2005)], our extended calculations predict that only very short hyperdeformed bands composed of a dozen discrete transitions *at the most* are to be expected–in contrast to the results known for the superdeformed bands. We stress the importance of the experimental research in terms of multiple-γ correlation analysis that proved to be very efficient for the superdeformation studies and seems very helpful in the even more difficult search for the discrete transitions in hyperdeformed nuclei.

DOI: 10.1103/PhysRevC.75.054304 PACS number(s): 21.60.Ev, 21.10.Re, 21.30.Fe, 27.60.+j

I. INTRODUCTION

The experimental search for nuclear high-spin hyperdeformation depends critically on two physically distinct steps: population of the very highly deformed nuclei, usually at relatively high temperatures of the order of 1 MeV or so, and detection of their presence through their electromagnetic decay, in the form of either "continuum radiation" or discrete radiation. However, the population of these highly exotic structures, although a necessary condition, does not yet guarantee their observability in terms of discrete γ lines. Consequently, it is not so much the *potential existence* of the hyperdeformed states predicted by quantum mechanics but both the *population of the highly elongated states at relatively high temperatures* *in a given experiment* and *the existence of the highly elongated states at low or zero temperatures in the studied nucleus* that determine the success or failure of the experimental identification through discrete γ lines. As argued later: too high a temperature or an incorrect choice of the angular momentum transfer to the compound nucleus *makes the population impossible*.

The most efficient experimental techniques that allow for large angular momentum transfers to populate very high-spins are heavy-ion reactions passing through high-temperature excitations of compound nuclei. This contrasts to the strategy followed in the theoretical studies of the hyperdeformation focusing so far on the search for the high-elongation shell-structures at zero temperatures (see, e.g., Ref. [1]). Unfortunately, there are no efficient techniques known to allow the population of hyper-deformed nuclei under the condition of vanishing nuclear temperature.

At high temperatures the shell effects underlying the existence of high-elongation structures are significantly weakened or absent and the population of such states becomes impossible. The exception to the rule is provided by the mechanism called Jacobi transition. According to this mechanism (cf. Refs. [2] and [3]), there may exist a narrow spin window, $[I_{\rm min}, I_{\rm max}]$ of a few $\hbar$ only, for which *the only deformations possible to populate* are very large ones—and this independently of the nuclear temperatures that may approach $T \sim 3$ MeV or so.

Within the nuclear mean-field, super- and/or hyperdeformations were predicted in many nuclei in several mass-regions [1,4–6]. However until now no convincing experimental evidence of discrete rotational states built on a hyperdeformed configuration had been reported.

Some years ago, an experiment on ^{108}Cd performed at Argonne National Laboratory reported evidence [7] of "very extended shapes" in a spin window ΔI of about 40 to 60$\hbar$. However, no direct theoretical interpretation was available and it remains unclear whether these data could be indeed connected to hyperdeformation. Subsequent analyses claimed that the data reported could not be associated with a hyperdeformed structure [8].

More recently five experiments were performed to study the γ decay following the formation of ^{128}Ba and ^{130}Xe compound nuclei at the highest spins, by the most efficient multidetector arrays available, Euroball IV in Strasbourg, EU, and Gammasphere in Berkeley and Argonne, USA. Preliminary results show the presence of rotational patterns of 3 or higher fold γ-ray coincidences in the form of the so-called Rotational Plane Mapped ridge structures in more than 10 different residual nuclei. All these nuclei have been rather cleanly selected by charged particle and/or discrete ground band γ-ray gating in addition to γ-fold gating, within the regions $Z = 52$–56 and $N = 52$–66 (cf. Refs. [9–14]). The corresponding dynamical moments $J^{(2)}$ (for more details see below) are directly extracted from the energy positions of these ridge structures for several nuclei. They are found in the range $J^{(2)} = 75$ to $125\hbar^2/\text{MeV}$, strongly indicating that both superdeformed (with say $J^{(2)} \sim 70\hbar^2/\text{MeV}$) or hyperdeformed (with $J^{(2)} \sim 110\hbar^2/\text{MeV}$) dynamical moments are present among these nuclei. The best candidates showing hyperdeformed structures so far are ^{124}Xe, ^{125}Cs, and ^{118}Te [14]. The analysis of these huge data sets, of the order of 5×10^{10} high-multiplicity events/run, is still in progress.

The purpose of the present article is a theoretical analysis of the nuclear hyperdeformation that accounts for the latest understanding of the problem with the decisive role of the Jacobi transition mechanism. We discuss the conditions of the formation and population of nuclear hyperdeformed configurations in the light of the most recent experimental results focusing on the role of Jacobi shape transitions in building up and *populating* hyperdeformed states. We believe that this particular aspect was overlooked in previous studies and can be held responsible for the current lack of experimentally observed discrete hyperdeformed states, providing today stringent criteria for the planning of future experiments. We also intend to stimulate the experimental effort by providing examples of large-scale calculations on nuclei under focus. The work presented here can be seen as the continuation of an analysis initiated in Refs. [2] and [3].

In the presentation of our results, we try to follow the sequence of events involved in the formation of very deformed configurations in nuclei followed by their decay. We thus recall in Sec. II some pertinent features of a fast-rotating liquid drop, the latter meant to simulate the high-temperature nuclear behavior. In particular, we discuss in detail various possible forms of manifestation of the Jacobi Shape transition that occurs at very high angular momentum in nuclei. Section III is devoted to the presentation of the theoretical framework. Our calculations are based on the macroscopic-microscopic approach and include the microscopic description of thermal excitations. The whole of Sec. IV is devoted to the detailed study of hyperdeformation in the mass $A \sim 130$ region. We present total potential energy curves from the high- to the low-temperature regime. These curves show the presence of three minima in all nuclei considered. In the third minimum, the so-called hyperintruder nucleonic orbitals are occupied, allowing us to associate it with the hyperdeformation. We calculate $J^{(2)}$ moments as functions of spin and compare them with the experimental data. Finally, we discuss the role of the hyperintruders in building up the moments of inertia. In Sec. V, we comment about hyperdeformation in other mass regions and discuss various options of designing the most appropriate experiments, before concluding in Sec. VI.

II. THE JACOBI SHAPE TRANSITION IN ATOMIC NUCLEI

The concept of Jacobi shape transitions was first introduced in the framework of gravitational systems. More than 40 years ago already, it was proposed that atomic nuclei, manifesting analogies in their behavior to that of a charged liquid drop, could also undergo a rapid change of shape at very high angular momentum [15]. In recent years several experiments probed this mechanism and the evidence exists now of the Jacobi transition both in light and medium mass nuclei [16,17]. As the temperature increases, the shell energies tend to vanish [18] and the liquid drop energy represents, to a good approximation, the high-temperature limit of the total energy of the nucleus.

We describe the nuclear surface using the spherical harmonics $Y_{\lambda\mu}(\theta,\varphi)$:

$$R(\theta,\varphi) = R_0 c(\{\alpha\})\left[1 + \sum_{\lambda}\sum_{\mu=-\lambda}^{\lambda} \alpha_{\lambda\mu} Y_{\lambda\mu}(\theta,\varphi)\right], \quad (1)$$

where $c(\{\alpha\})$ factor accounts for the conservation of the nuclear volume and $R_0 = 1.2A^{1/3}$ fm. Here, $\{\alpha \equiv \alpha_{\lambda\mu}\}$ stands for the full set of deformation parameters. In what follows, we shorten the notation for the axial deformation parameters to $\beta_\lambda \equiv \alpha_{\lambda,0}$.

The liquid drop energy is parametrized with the help of the Lublin-Strasbourg Drop (LSD) of Ref. [19]. The energy of a rotating liquid drop can be written down as

$$E(I;\{\alpha\}) = E_0(\{\alpha\}) + \frac{I(I+1)}{2J_{\text{macro}}(\{\alpha\})}, \quad (2)$$

where $E_0(\{\alpha\})$ is the static energy according to Ref. [19] and where $J_{\text{macro}}(\{\alpha\})$ stands for the moment of inertia of a rigid body. The results of a minimization over deformation space including (β,γ) quadrupole deformation and β_4, β_6, and β_8 deformations are shown in Figs. 1 and 2 illustrating the Jacobi transition in the nucleus ^{152}Dy.

The Jacobi transition is a rapid (in terms of the spin increase) change in the equilibrium shapes that occurs at high angular momentum. In Figs. 1 and 2, one can see that up to spin $I \sim 70\hbar$, the equilibrium deformations of the liquid drop correspond to oblate shapes and that between $I \sim 70\hbar$ and $I \sim 78\hbar$, the ^{152}Dy nucleus changes its shape arriving at a new equilibrium that corresponds to a strongly prolate shape. In a very narrow spin window of $\Delta I \approx 6\hbar$ centered at $I_0 \approx 76\hbar$ all ^{152}Dy nuclei populated at a high temperature range of $T > 1$ MeV will reach the equilibrium at deformations $\beta_2 \sim 0.4$–0.9, i.e., between the super- and the hyperdeformation no matter the details of the nuclear formation process.

According to Fig. 2 the fission barrier at $I = 78\hbar$ amounts to about 2.5 MeV. This value is reduced to nearly 0.5 MeV when the multipoles $\lambda > 8$ are taken into account in the minimization procedure and although the corresponding classical system formally would still be stable, this is far from being true for the nuclear quantum systems that are expected to fission. At $I \sim 72$–$76\hbar$ where the feeding of the superdeformed yrast band begins according to experiment, the minimum of the energy is around $\beta_2 \sim 0.6$. This implies that the population is maximal at the superdeformed configurations provided the experiment reaches the narrow spin window of $\Delta I \equiv [72, 76]\hbar$.

From the existence of fission isomers in actinide nuclei we know that barriers of about 2 MeV are sufficient to stabilize these isomers. We conclude that fission barriers of the order of 2 MeV may be sufficient to stabilize other highly deformed nuclei. The corresponding spin at which the fission barrier is about 2 MeV (∼4 MeV on our maps that do not contain multipoles with $\lambda > 8$) is $I \sim 74\hbar$. For the ^{152}Dy nucleus, the spins of the yrast superdeformed band are known [20]

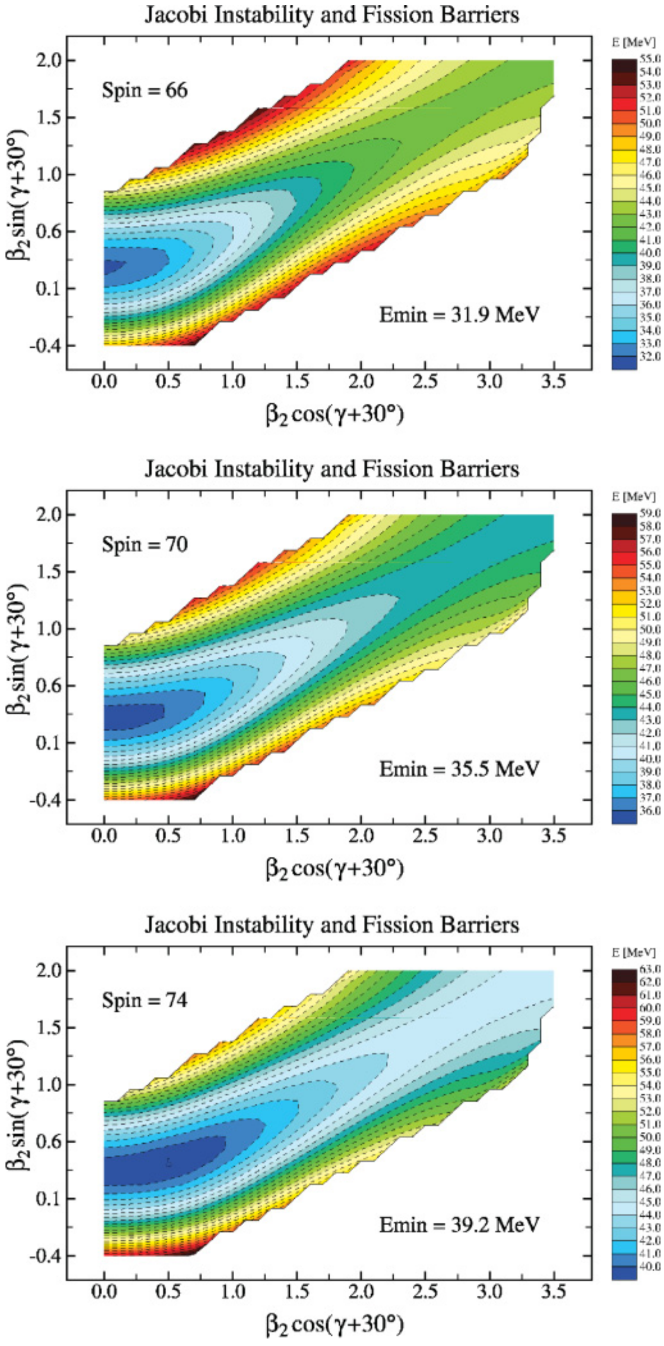

FIG. 1. (Color online) Total energy surfaces in ^{152}Dy illustrating the Jacobi shape transition mechanism. For given (β_2, γ), minimization includes β_4, β_6, and β_8 deformations.

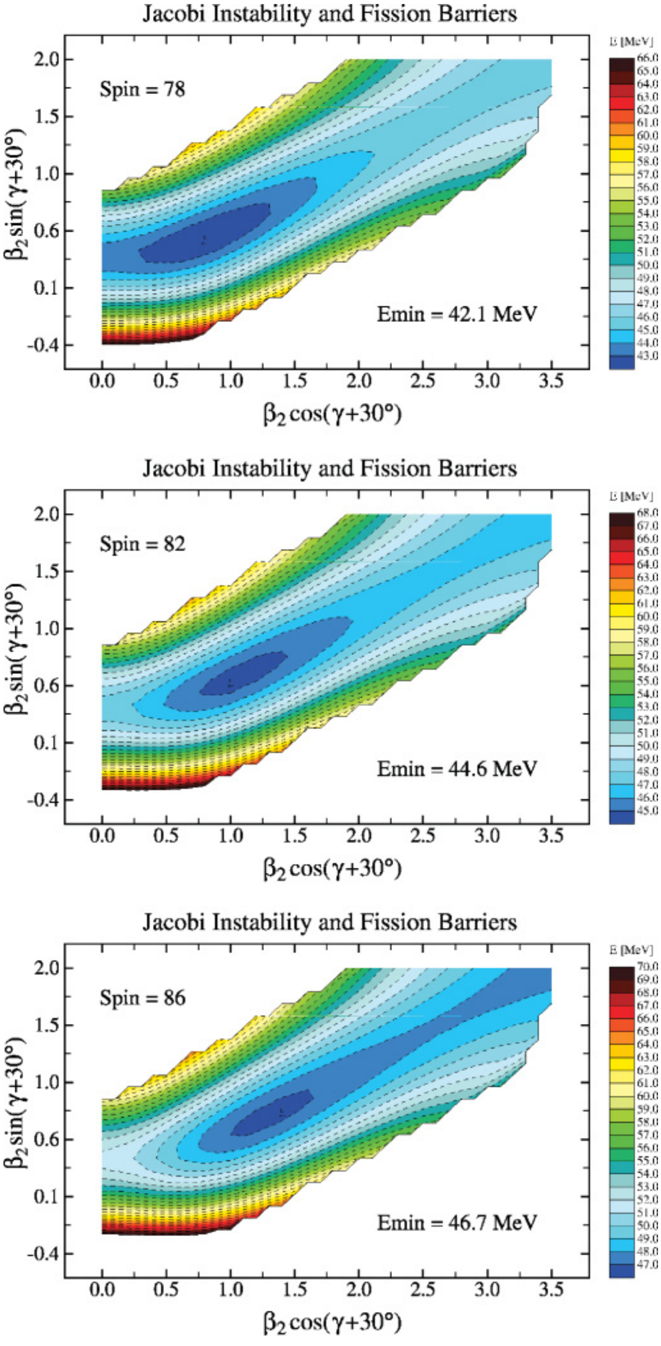

FIG. 2. (Color online) Similar to Fig. 1 for $I = 78$–$86\hbar$.

up to $66\hbar$ and it is expected that the highest-spin states are fed through about four statistical transitions of the average multipolarity $1.5\hbar$. We may thus expect that the highest spin state of $I = 66\hbar$ is fed from some excited states at $I \sim 72\hbar$, i.e., at $\beta_2 \sim 0.5$–0.7 according to the results in Figs. 1 and 2. From the fact that the $I = 68\hbar$ state has not been seen in experiment, we may deduce that the barrier of ~ 4.0 MeV as predicted by the result for $I = 74\hbar$ in Fig. 1 (or about 2 MeV when the multipoles $\lambda > 8$ are taken into account) is at the limit of fission stability. This may be considered consistent with the results for the fission isomers in the actinide nuclei as mentioned above—and this comparison may be taken as a provisional (until the experimental fission lifetimes become known) "unit" of fission stability that could be used to interpret further theoretical results related to the barrier heights within the present approach.

In early references, i.e., Refs. [1,6], predictions of the existence of hyperdeformed shapes were based on zero-temperature mean-field calculations. At that time the superdeformed nuclei had been populated in experiments with a certain "easiness" and it had been expected that similar types of experiments would provide the results for hyperdeformed nuclei although, perhaps, at lower statistics. As it seems today, the physics behind the population of hyperdeformed states does involve similar mechanisms (importance of the thermal excitations and of the Jacobi transitions together with the shell gaps at large deformations)—but these mechanisms combine in quantitatively different ways leading to differences in the expected experimental results. In particular the simultaneous presence of the hyper- and superdeformed gaps in the single-particle spectra in some nuclei deters the survival of the hyperdeformed minima because of decay from the hyper- to the superdeformed configurations. Most of the superdeformed nuclei found up to now experimentally together with their mother nuclei are populated *at those same spins where the Jacobi shape transition takes place*, according to the calculations. In this sense the success of the whole program of the superdeformation studies can be seen a result of a lucky coincidence: All these very deformed nuclei, whose *existence* is assured by the zero-temperature shell effects, could be *populated* through the high-temperature intermediate-states because the Jacobi transition happened to be present in those nuclei at those spins, as predicted today by the LSD model.

It then becomes clear that this argument must also be valid in the case of hyperdeformation: To maximize the chances of populating hyperdeformed states and observing discrete transitions, candidate nuclei must be selected in part with regard to the properties of their Jacobi shape transition. In this respect, the situation encountered in ^{152}Dy does not appear to be favorable: indeed, in the deexcitation phase, when shell effects progressively arise, the presence of two large superdeformed shell gaps at $Z = 66$ and $N = 86$ drives the nucleus into a superdeformed energy minimum. The γ decay then proceeds via fast stretched $E2$ transitions characteristic of the superdeformed rotational bands in this region. Moreover, we know from experiment that in the spin window $\Delta I \equiv [72, 76]\hbar$, normal-deformed and superdeformed states are populated in (HI,*xn*) reactions in ^{152}Dy, but no hyperdeformed states. Theoretically, in reference to Figs. 1 and 2, this corresponds to the situation where the location of the shallow minimum in the potential energy surface corresponds to elongations of $\beta_2 \sim 0.5$. At spins $I \sim [78, 82]\hbar$, the Jacobi transition is completed, and the location of the minimum has shifted toward larger elongations of the order of $\beta_2 \sim 1.1$. It seems natural to think that the probability of populating hyperdeformed states should be maximal for $I \sim [78, 82]\hbar$. However, as we mentioned earlier the fission barrier at this spin range vanishes. Consequently, it is very unlikely that one may be able to populate a hyperdeformed minimum in ^{152}Dy by (HI,*xn*) reactions, even if such a minimum can exist at lower temperatures as suggested in Refs. [4] and [6].

In contrast, the results for ^{122}Xe nucleus illustrated in Fig. 3 look much more promising. This nucleus cumulates a number of advantages: (i) It undergoes a very clear Jacobi shape transition starting at a relatively low spin, $I_{\rm crit} \sim 70\hbar$. (ii) After the Jacobi transition has occurred, the nucleus possesses a stable prolate minimum that is deeper (as compared to the one in ^{152}Dy) and well-defined, corresponding to a significantly larger deformation of $\beta_2 \sim 0.9$ at $I \sim 76\hbar$. (iii) The fission barrier is still of the order of $B_{\rm fiss} = 8$ MeV at $I \sim 80\hbar$. We convinced ourselves that including higher order multipole deformations up to $\lambda \leqslant 16$ does not lower this fission barrier by more than about 2 MeV.

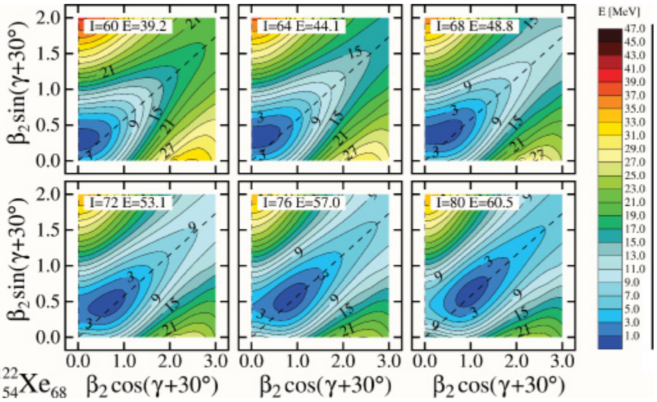

FIG. 3. (Color online) Total energy surfaces in ^{122}Xe from the LSD calculations illustrating another scenario of the Jacobi shape transition. All the isotopes of Te, I, Xe, Cs, and Ba considered in this paper are characterized by a relatively deep prolate minimum for $\beta_2 \geqslant 0.9$ or so. It takes about 10–16 $\hbar$ extra before the fission barrier vanishes.

One arrives at the following qualitative observation: only the nuclei that manifest a Jacobi shape transition associated with large fission barrier may give us a chance to *populate* states corresponding to very extended shapes by means of the standard (HI,*xn*) reactions. More precisely, the results shown in Fig. 3 illustrate that, at sufficiently high spins, there exists only *one* minimum available for the compound nucleus—that corresponding to very extended shapes. From Figs. 1 and 2, the minima in ^{152}Dy at $I \sim 76\hbar$ are very shallow and therefore suggest that *a priori* all shapes ranging from normal deformation ($\beta_2 \sim 0.3$) to superdeformation ($\beta_2 \sim 0.6$) and eventually hyperdeformation ($\beta_2 \sim 1.0$) may be populated with similar probabilities at high temperatures that are usually reached in the (HI,*xn*) reactions.

Let us emphasize that predictions of the existence of the hyperdeformed nuclei *at the zero temperature limit*, Ref. [1], as well as the systematic predictions of Ref. [6], remain valid. The main obstacle in populating them are all those nuclear reactions that lead to high-spin states *at high temperatures only*. Should there be a way of populating $I \sim 70$–$80\hbar$ states in, e.g., Hf and Yb nuclei at near zero temperatures the hyperdeformed states predicted there should be, in principle, observed as well.

III. EXTENDED MACROSCOPIC-MICROSCOPIC APPROACH

To go beyond the pure macroscopic picture of nuclei, a description of quantum effects must be incorporated. The phenomenological so-called macroscopic-microscopic approach provides an effective framework that is also well-suited to large-scale calculations. A disadvantage of this method is the necessity of predefining the deformation space. The latter remains fixed in the corresponding deformation-mesh calculations. We have added the option of automatic deformation minimization, which brings us somewhat closer to the self-consistent type schemes. In our case we combine the deformation-mesh technique, in particular for the calculation of macroscopic energy landscapes, and the automatic minimization in large-deformation spaces when shell and thermal effects are fully taken into account.

The macroscopic-microscopic techniques rely on the decomposition of the total energy of the nucleus into the sum of several terms, depending on the degree of refinement requested. In its simplest form,

$$E_{\text{total}}(\{\alpha\}) = E_{\text{LD}}(\{\alpha\}) + E_{\text{shell}}(\{\alpha\}), \tag{3}$$

where $E_{\text{LD}}(\{\alpha\})$ represents the energy of a deformed nuclear liquid drop characterized by a set of deformation parameters $\{\alpha\}$, e.g., $\{\alpha_{\lambda\mu}\}$ in Eq. (1). Quantal effects are taken into account by the shell energy, $E_{\text{shell}}(\{\alpha\})$. The procedure to calculate this quantity is well-established and originates from the early works of Strutinsky [21]. It requires as input the nucleonic single-particle levels. In our calculations, the latter are obtained by diagonalizing the Woods-Saxon Hamiltonian with the so-called Universal parametrization of Ref. [22]. We use the Cartesian, deformed, anisotropic harmonic-oscillator basis with up to 22 N shells and basis cutoff $N_c \sim 600$, assuring the stability of the final result when adding new basis states.

Nuclear rotation is described using the cranking model. Most of the formalism used in this article is presented in detail in Ref. [6]; we limit ourselves to the definitions only. The cranking Hamiltonian reads

$$\hat{h}^{\omega} = \hat{h}_0 - \hbar\vec{\omega} \cdot \hat{j}, \tag{4}$$

where $\hat{h}_0$ is the static, i.e., nonrotating Hamiltonian, $\vec{\omega}$ is the rotational frequency vector (according to our convention rotation takes place about the x axis of the body-fixed frame), and $\hat{j}$ the single-particle angular momentum vector (operator). The diagonalization of Eq. (4) provides the single-particle eigenvalues and wave functions in the rotating frame.

For rotating nuclei decomposition, Eq. (3) must be slightly adapted. In the first step, the total Routhians, i.e., energies in the rotating frame $R_{\text{LD}}(\{\alpha\};\omega)$ and $R_{\text{shell}}(\{\alpha\};\omega)$ are calculated. The transformation from the rotating to the laboratory frame, and from the rotational frequency representation to the angular momentum representation, is achieved by the canonical transformation

$$E(\{\alpha\}; I) = R_{\text{LD}}(\{\alpha\};\omega(I)) + R_{\text{shell}}(\{\alpha\};\omega(I)) + \vec{\omega} \cdot \vec{I}. \tag{5}$$

The procedure involves several technicalities that we shall not cover here as a comprehensive presentation of them can be found in Refs. [6] and [23].

When dealing with highly excited nuclei it is important to include in the formalism the possibility of describing thermal effects that originate from the excitation energy of the compound system. For this purpose, the total Routhian at temperature T is written as

$$\begin{aligned} R_{\text{total}}(\{\alpha\};\omega,T) \;=\; & R_{\text{LD}}(\{\alpha\};\omega,T) + R_{\text{shell}}(\{\alpha\};\omega,T) \\ & + R_{\text{therm}}(\{\alpha\};\omega,T), \end{aligned} \tag{6}$$

with an extra term, $R_{\text{therm}}(\{\alpha\};\omega,T)$, which is defined as usual by

$$R_{\text{therm}}(\{\alpha\};\omega,T) = \sum_i \left[n_i^{\omega}(T) - n_i^{\omega}(T=0)\right] e_i^{\omega}, \tag{7}$$

where $\{e_i^{\omega}\}$ are the single-particle Routhians at the rotational frequency ω and $n_i^{\omega}(T)$ are the occupation probabilities of the single-particle Routhians at temperature T,

$$n_i^{\omega}(T) = \frac{1}{1+\exp\left[\left(e_i^{\omega}-\lambda\right)/T\right]}. \tag{8}$$

Above λ is the Fermi level at the temperature T. The total Routhian contains two analogous shell- and thermal-energy expressions for both kinds of nucleons. A comprehensive presentation of the formalism describing thermal excitations that we adopted can be found in Ref. [24].

An appropriate treatment of such thermal excitations in nuclei requires the definition of the total nuclear excitation energy E^* first. This quantity represents the total energy available to the system, i.e., available for distribution over all nucleons within the pre-supposed modes of excitation. In our case this energy splits into deformation-, rotation-, and thermal-contributions. Here we did not take into account the possibility for the liquid drop itself to generate an additional entropy, as the temperatures involved ($T \sim 2$ MeV) are believed to be too small for this effect to be significant. Therefore the liquid drop model parameters are kept temperature independent and no extra term is added to the Hamiltonian (4) on the account of the macroscopic-energy temperature-dependence.

The temperature is determined locally at each deformation $\{\alpha\}$ and total angular momentum I from a given excitation energy E^*. For this purpose, the total free Routhian F_R defined as

$$F_R = R_{\text{total}}(\{\alpha\};\omega,T) - T \cdot S(\{\alpha\};\omega,T) \tag{9}$$

is calculated for the deformations $\{\alpha\}$ on a mesh of rotational frequency points $\{\omega_k\}_{k=1,\ldots,n}$ and temperature points $\{T_l\}_{l=1,\ldots,m}$. In Eq. (9), the total Routhian R_{total} is given by Eq. (6) and $S(\{\alpha\};\omega,T)$ stands for the entropy calculated as in Ref. [24]. Using a linear interpolation of the total Routhian (6) over the rotational frequency at the deformations $\{\alpha\}$, we extract the total energy of the system $E(\{\alpha\},I,T)$ at given angular momentum I and temperature T. For given excitation energy E^*, we obtain the *local* temperature, which depends on the equilibrium deformations $\{\alpha\}$ and the angular momentum I, after solving the equation

$$E_{\text{total}}(\{\alpha\},I,T) = E^* \tag{10}$$

through a quadratic interpolation of the total energy over the temperature T. The pertaining quantity to explore potential energy landscapes for hot rotating nuclei is then the total free energy defined as

$$F_{\text{total}}(\{\alpha\},I,E^*) = E_{\text{total}}(\{\alpha\},I,T) - T \cdot S, \tag{11}$$

where both temperature T and entropy S are the quantities depending on the actual deformation $\{\alpha\}$, excitation energy E^*, and total angular momentum of the system.

The macroscopic-microscopic method as succinctly presented was implemented together with a minimization algorithm based on the conjugated gradient method. The total free Routhian (9) is a function of the deformation parameters $\{\alpha \equiv \alpha_{\lambda\mu}\}$. Our calculations took into account four deformation degrees of freedom that we checked play the most prominent role in very elongated systems: β_2, β_4, β_6, and β_8. The additional effect of triaxiality is discussed later in Sec. IV B. For a fixed elongation β_2 ranging from 0 to 3.0 by steps of 0.1, and on the mesh of rotational frequency $\{\omega_k\}_{k=1,\ldots,n}$ (whose range depends on the deformation considered) and temperature $\{T_l = 0, 0.5, \ldots, 3 \text{ MeV}\}$, the total free Routhian was minimized with respect to β_4, β_6, and β_8. The minimization used as a starting point the estimates of the equilibrium deformations obtained within the pure macroscopic approach, which has the advantage of being a much smoother surface of the deformation parameters.

IV. HYPERDEFORMATION IN $A \sim 130$ NUCLEI

As outlined in the Introduction, one of the most promising areas to investigate hyperdeformation is the mass $A \sim 130$ range for the Te, I, Xe, Cs, and Ba isotopes. This region was the subject of five experiments with Euroball IV (2001) and Gammasphere (2003). Partial results were published in Refs. [9–14]. These experiments were motivated by the existence of very neat and stable Jacobi shape transitions like those shown in Fig. 3 and by the so-called Ultimate Cranker calculations [25].

This series of experiments provides for the first time a set of quantitative data that can be used to test theoretical predictions. We therefore paid particular attention to this mass region and studied in detail the following isotopes: $Z = 52$, ^{118}Te; $Z = 53$, ^{121}I; $Z = 54$, ^{124}Xe and ^{126}Xe; $Z = 55$, ^{125}Cs; and $Z = 56$, ^{126}Ba and ^{128}Ba. For all of them, the $J^{(2)}$ moments were extracted from the ridge structure analysis and an estimate of the number of statistical bands and of the angular momentum is also available [9–14]. In our calculations, we found that all of the aforementioned isotopes presented many similar features, in particular: (i) their potential energy curves show the same three-minimum profile, (ii) their microscopic structure involves the same nucleonic super- and hyperintruder orbitals, and (iii) their theoretical moments of inertia have nearly the same values. For these reasons, and to keep this article a moderate length, we have chosen to present only a few selected figures illustrating the most important issues.

A. Multidimensional total energy calculations

We wish to obtain information about the evolution of the hyperdeformed nuclear configurations as a function of spin and temperature as well as about barriers separating those minima from other shape-competing minima and/or from the fission channel.

Figure 4 shows the total free energies of ^{122}Xe as a function of the elongation parameter $(=\alpha_{20})$ at an excitation energy $E^* = 70$ MeV and for the angular momenta $I = 50, 60, 70, 80\hbar$. The choice of this particular value of the excitation energy aims at simulating the nuclear conditions at the high-temperature regime.

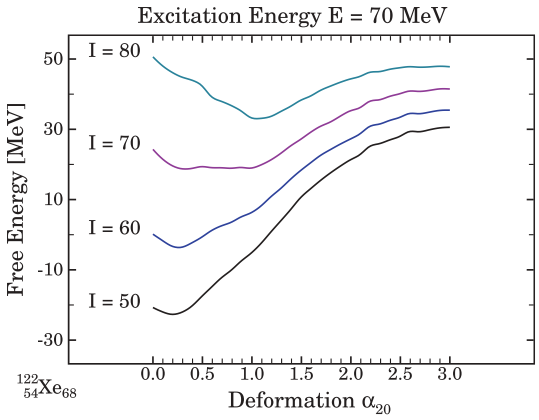

FIG. 4. (Color online) Total free energy of ^{122}Xe nucleus as a function of the elongation $\alpha_{20} \equiv \beta_2$ at a fixed excitation energy $E^* = 70$ MeV. At each elongation point $\beta_2 = 0.0, \ldots, 3.0$, $\Delta\beta_2 = 0.1$, each rotational frequency ω, and each temperature T, the total free Routhian is minimal with respect to β_4, β_6, and β_8.

Not surprisingly, the nuclear free energy varies very smoothly with respect to deformation showing a trend characteristic of a liquid drop. In fact, Fig. 4–where shell and thermal effects are taken into account–can be linked to Fig. 3, where only the liquid drop energy is plotted. It justifies *a posteriori* the approximation of a pure liquid drop behavior at high temperatures. We notice that at angular momenta $I > 70\hbar$, the energy profile shows a neat and unique minimum corresponding to very large elongations of the order of $\beta_2 \sim 1.0$. This is a possible candidate for an experimental hyperdeformation study.

The next three illustrations in Fig. 5 model the gradual appearance of the shell effects that accompanies the cooling of the nucleus as the γ emission proceeds and the spin decrases. With increasing shell effects two additional distinct minima show up: a normal deformed one corresponding to elongations of about $\beta_2 \sim 0.3$ and a superdeformed one with $\beta_2 \sim 0.7$. All the other isotopes considered present very similar energy patterns.

At spin $I \sim 70\hbar$ and for temperatures $T \sim 0.5$ MeV (Fig. 5, bottom frame), the hyper-deformed minimum is still yrast. The fission barrier is $\sim$9 MeV large, and the barrier between the superdeformed and this minimum is $\sim$3.5 MeV. It is not clear yet whether under realistic experimental conditions a nucleus could be populated at such a high spin and (relatively) low excitation energy. In other words, the evaporation of particles (protons, neutrons, or alpha particles) involves a significant loss of angular momentum and excitation energy. When the decay proceeds only via emission of γ rays, the spin of the nucleus might already be too low for a hyperdeformed configuration: at $E^* = 50$ MeV and $I = 60\hbar$, the hyperdeformed minimum has practically disappeared and only the normal-deformed states can be populated. It turns out the hyperdeformed bands are expected to be extremely short, 5 to 10 transitions at most, as compared to over 30 transitions in many superdeformed bands.

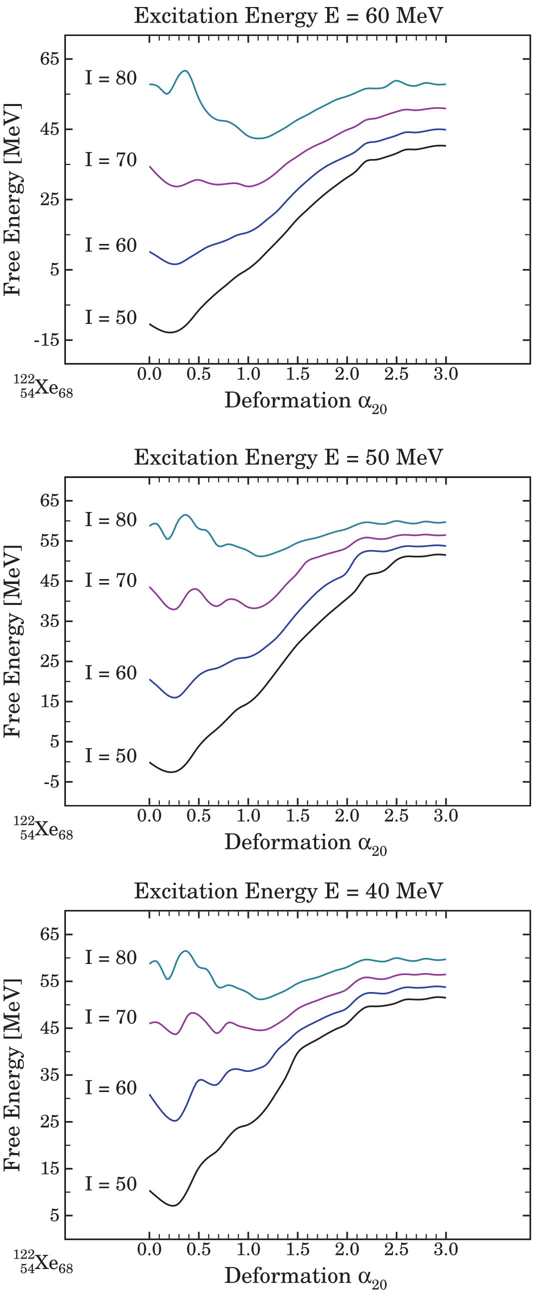

FIG. 5. (Color online) Same as Fig. 4 for excitation energies $E^* = 60$, 50, and 40 MeV.

B. Effect of triaxiality

The results shown in Figs. 4 and 5 assume axial symmetry for the nucleus in question. However, it is known that for moderate deformations at least, triaxiality may play an important role. Moreover, the Jacobi transition is characterized by a triaxial regime, although in a very short window of angular momenta only. In this section, we illustrate the possible role of triaxiality in the mass $A \sim 120$ nuclei.

Figure 6 shows the example of the total free energy of ^{126}Xe as a function of its elongation β_2 at a fixed excitation energy $E^* = 55$ MeV and angular momentum $I = 75\hbar$ near the Jacobi transition regime, i.e., where the effect of triaxiality is the strongest. The solid line shows the result for axial symmetry, where the total free Routhian is minimized as a function of β_4, β_6, and β_8 for each point β_2, with $\gamma = 0$. The dashed line corresponds to the minimization with the γ angle included. Figure 7 shows the evolution of the degree of triaxiality γ as a function of the elongation β.

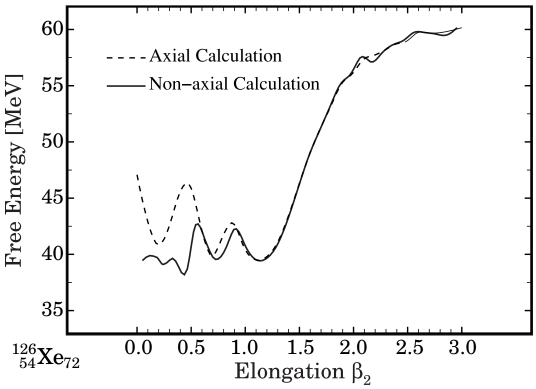

FIG. 6. Total free energy of the ^{126}Xe nucleus as a function of the elongation β_2. This is an "academic case" representation illustrating the role of triaxiality for other parameters fixed: here $E^* = 55$ MeV and $I = 75\hbar$. Dashed and solid lines represent axial and nonaxial configuration results, respectively. Triaxiality is parametrized by the γ angle and is included in the minimization of the energy.

Two observations can be made. First, the energy curve with triaxiality is always lower or equal to the curve without–enlarging the deformation space can only improve the quality of the description and lower the total energy. The second observation, important because it's not an obvious result, is that the effect of triaxiality occurs mostly at relatively moderate deformation, corresponding to the normal-deformed and superdeformed shapes. For larger deformations of the order of $\beta_2 > 0.8$, there is very little admixture of triaxiality in the ^{126}Xe nucleus.

Similar calculations performed in nuclei of this mass region give the same results and confirm that the role of triaxiality is mostly confined to moderate deformations. Although this means that the relative probabilities of population of the

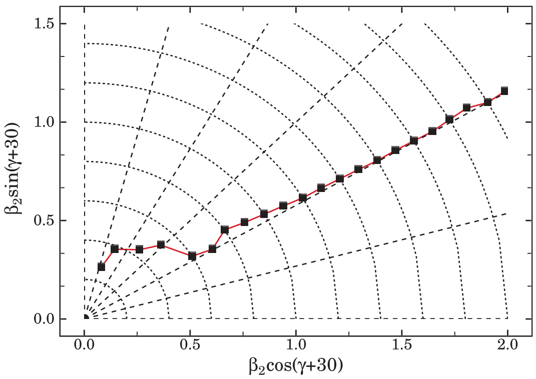

FIG. 7. (Color online) Evolution of the shape in the (β, γ) plane for the nonaxial configuration of Fig. 6; auxiliary straight lines are placed at $\Delta\gamma = 15^\circ$.

normal-deformed (ND) minimum on the one hand, and the superdeformed (SD) and hyperdeformed (HD) minima on the other, may be altered; it also suggests that triaxiality should not be expected to play a major role in the *occurence* of hyperdeformation. In particular, it does not destroy the barriers between the SD and HD minima well, nor does it influence the energy of the hyperdeformed minimum or the height of the fission barrier.

C. Hyperintruder levels and hyperdeformation

Presently there is a relatively wide consensus as to what criteria should be used to define hyperdeformation. Any argument based on the absolute values of the deformation parameters or geometrical axis-ratios depends on the particular parametrization of the nuclear surface and can therefore not pretend to be universal. A better criterion is provided by the concept of intruder orbitals. It is known that in spherical or normal-deformed nuclei, single-particle levels originating from a spherical mean-field shell $N_{\text{sph}} + 1$ with the maximum angular momentum $j = (N_{\text{sph}} + 1)/2$ are pushed down into the shell N_{sph} because of the strong spin-orbit interaction. Similarly, it was demonstrated that in superdeformed nuclei, the additional effect of the large quadrupole deformation resulted in a shell N_{SD} containing a *superintruder* coming from shell $N_{\text{sph}} = N_{\text{SD}} + 2$ as well as the "extruder" levels originating at $N_{\text{sph}} = N_{\text{SD}} - 1$. It was therefore suggested that hyperdeformation should be defined by an analogous criterion, namely, a shell N_{HD} should contain a *hyperintruder* originating from shell $N_{\text{sph}} = N_{\text{HD}} + 3$, possibly "hyperextruders" originating from $N_{\text{sph}} = N_{\text{HD}} - 2$ (cf. Ref. [26]).

This definition presents the advantage of relying only on pure quantum mechanical arguments. Moreover, numerous studies of superdeformation showed that the properties of the superdeformed bands were highly sensitive to the presence of the superintruder orbitals (which in addition happen to carry a large angular momentum).

In the $Z > 50$ nuclei of the mass region $A \sim 120$–130, the hyperintruders are $N_{\text{sph}} = 7$ orbitals sloping down into the $N_{\text{HD}} = 4$ shells. In Figs. 8 and 9 we show the single-particle Routhians for both the protons and the neutrons in ^{122}Xe as function of the rotational frequency. They were calculated at the deformation corresponding to the very extended 3rd minimum shown in Figs. 4 and 5. More precisely, we set $\beta_2 = 1.1, \beta_4 = 0.18, \beta_6 = -0.02$, and $\beta_8 = -0.02$, corresponding to the deformations that minimize the total free Routhian at $I \sim 75\hbar$. In Fig. 8, the level labeled by [770]1/2 originates from $N_{\text{sph}} = 7$ and is driven down into a bunch of levels that all come from the spherical main shell $N_{\text{sph}} = 4$. Similarly, in Fig. 9, the level labeled by [770]1/2 (at approximately −4.5 MeV, on the left) is also an $N_{\text{sph}} = 7$ orbital sloping down and mixing with the $N_{\text{sph}} = 4$ shell levels. All these hyperintruder levels are occupied in ^{122}Xe for $\omega \geqslant 0.45$ MeV. The corresponding, very extended minimum is therefore indeed a hyperdeformed minimum. Similar results are obtained for the neighboring isotopes of $^{118}_{52}$Te, $^{121}_{51}$I, $^{124}_{54}$Xe, $^{126}_{54}$Xe, $^{125}_{55}$Cs, $^{126}_{56}$Ba, and $^{128}_{56}$Ba, even though β_2 in the hyperdeformed minimum varies from one isotope to another ($\beta_2 \sim 0.9$ for ^{118}Te to $\beta_2 \sim 1.2$ in ^{126}Ba).

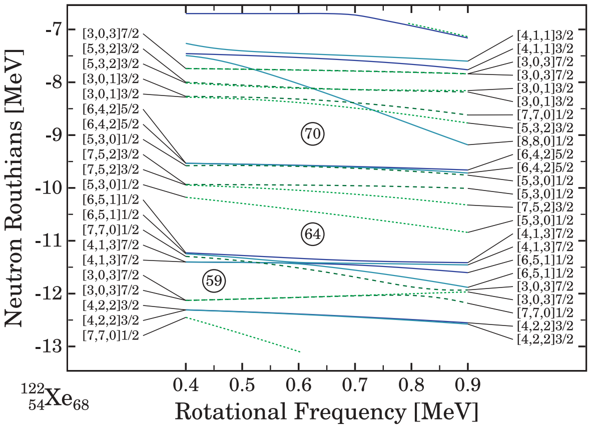

FIG. 8. (Color online) Neutron single-particle Routhians in ^{122}Xe. For deformation, see text. The curves are labeled by the Nilsson labels. The hyperintruder orbital is [770]1/2.

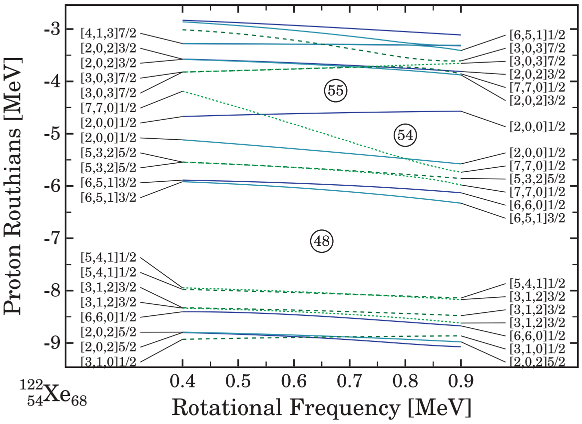

FIG. 9. (Color online) The same as in Fig. 8 but for proton single-particle Routhians. The hyperintruder orbital is [770]1/2.

D. Moments of inertia in hyperdeformed $A \sim 130$ isotopes

From the calculations presented in Sec. III, it is relatively simple to derive the theoretical kinematical moments of inertia $J^{(1)}$ and the dynamical moments $J^{(2)}$. They are defined as usual by the expressions

$$J^{(2)} = \frac{dI}{d\omega} \quad \text{and} \quad J^{(1)} = \frac{I(\omega)}{\omega}. \tag{12}$$

We assume that the cranking axis coincides with the x axis of the body fixed reference frame; the corresponding total angular momentum reads

$$I(\omega) \approx I_x(\omega) = \sum_{i \in \{\text{conf}\}} \langle \varphi_i^\omega | \hat{j}_x | \varphi_i^\omega \rangle, \tag{13}$$

where {conf} denotes the ensemble of single-particle levels that are occupied. The $|\varphi_i^\omega\rangle$ are the single-particle Routhian wave functions at the rotational frequency ω. Obviously, the Routhians and angular momentum depend also on the deformation.

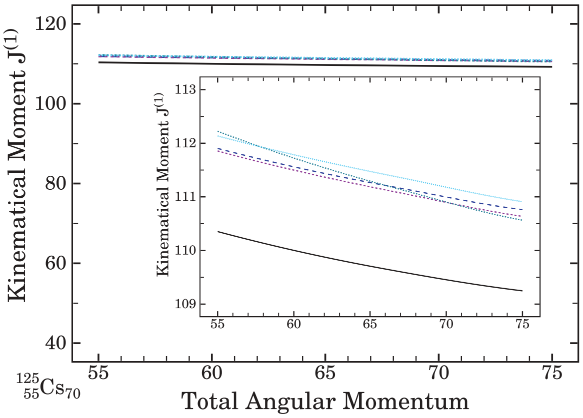

FIG. 10. (Color online) Kinematical moments of inertia in ^{125}Cs at $T = 0$ for the five lowest particle-hole excitations built on the vacuum configuration in the hyperdeformed minimum as a function of the angular momentum. The elongation is fixed at $\beta_2 = 1.1$. Other deformations are readjusted automatically as a function of the rotational frequency so as to minimize the total free Routhian. The inset frame shows a magnification of the vertical scale.

Figures 10 and 11 show an example of the calculations of the kinematical and dynamical moments in the case of ^{125}Cs. The total spin and the moments of the five lowest particle-hole excitations built on the vacuum configuration in the hyperdeformed minimum are calculated on a mesh of rotational frequencies $\{\omega_k\}_{k=1,\ldots,n}$. In this nucleus, the elongation in the hyperdeformed minimum is $\beta_2 = 1.1$. The other deformation parameters β_4, β_6, and β_8 are automatically readjusted so as to minimize the total free Routhian for the vacuum configuration. By interpolation over the ω_k, we obtain the curves of the moments of inertia as a function of the angular momentum.

Both plots in Figs.10 and 11 show that all the particle-hole configurations considered here have nearly the same moments of inertia. This is consistent with the preliminary results from the ridge structure analysis in these nuclei [14] which suggests the existence of five to ten bands in a given ridge structure.

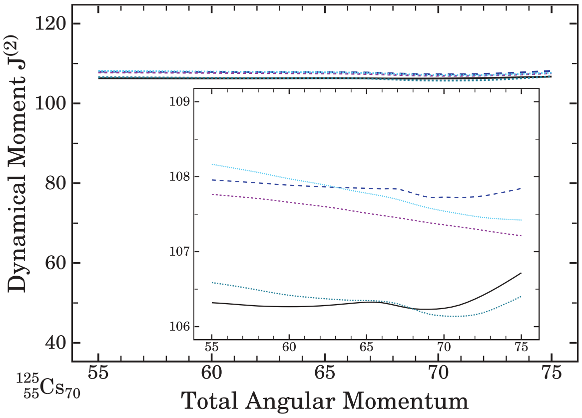

FIG. 11. (Color online) Dynamical moments in ^{125}Cs at $T = 0$ for the five lowest particle-hole excitations built on the vacuum configuration in the hyperdeformed minimum as a function of the angular momentum. Same configurations as in Fig. 10.

TABLE I. Dynamical moments $J^{(2)}$ averaged over the spin range $55\hbar \leqslant I \leqslant 75\hbar$ in several isotopes of the mass $A \sim 130$ region. The results shown in the first line were obtained in the HD minimum and involve the occupation of the proton $N_{\rm sph} = 7$ and neutron $N_{\rm sph} = 7$ single-particle orbitals. The line marked $J_{\rm rig}$ gives the equivalent rigid-body moments while the last line marked $J^{(2)}_{\rm exp}$ gives the experimental moments as extracted from the ridge structure analysis. The uncertainty of the latter is $\pm 8\hbar^2$ MeV^{-1} [14].

Nucleus	^{118}Te	^{121}I	^{122}Xe	^{124}Xe	^{125}Cs	^{126}Xe	^{126}Ba
$J^{(2)}$	97.0	102.0	108.0	111.0	108.0	110.0	118.0
$J_{\rm rig}$	92.7	97.3	106.7	109.9	111.6	117.7	122.4
$J^{(2)}_{\rm exp}$	111.0	77.0	77.0	111.0	100.0	83.0	77.0

Let us note that the theoretical differences between the $J^{(2)}$ moments of various particle-hole configurations (visible in the inset frame) are far below the present experimental uncertainty of about $\pm 8\hbar^2$ MeV^{-1}.

Similar calculations were performed in the other nuclei of this mass region. In all the cases studied, the dynamical moments of various particle-hole excitations show the characteristic trend to cluster around a mean value and to change very little with the angular momentum in the window $55\hbar \leqslant I \leqslant 75\hbar$. Because of this near "degeneracy" and very small fluctuations, we can present the result in the form of an average moment for each isotope (see Table I). Observe that the moments of inertia of all these nuclei lie very close to each other.

Table I reports for comparison also the rigid-body moments of inertia calculated at the hyperdeformed minima at spin $I = 75\hbar$. In the lighter isotopes, the elongation in the hyperdeformed minimum is about $\beta_2 \sim 1.0$, whereas it is about 20% larger in the heaviest isotopes with $\beta_2 \sim 1.2$. The moments were calculated with the radius of the mass distribution equal to $R = r_{\rm cen} A^{1/3}$ fm, where $r_{\rm cen}$ is the radius of the central Woods-Saxon potential as in Ref. [22]. We notice that most of these nuclei behave very much like rigid rotors, as happens in some of the superdeformed bands, e.g., of the rare-earth region.

The results in Table I suggest that in four nuclei, i.e., ^{121}I, ^{122}Xe, ^{126}Xe, and ^{126}Ba, the hyperdeformed configurations, though present theoretically, were not observed in the discussed experiments.

The free energy patterns shown in Figs. 4 and 5 also suggest that at spins of $I \sim 70\hbar$ and excitation energies of 40–50 MeV, superdeformed bands built on the second minimum, for an elongation of $\beta_2 \sim 0.6$–0.7, could be populated. When calculated in the superdeformed well, the moments of inertia range from 60 to $80\hbar^2$ MeV^{-1}, depending on the isotope. They appear thus markedly different, being lower by 20–30% compared to the hyperdeformed minimum. We discuss this point in the next section.

E. Discussion of the role of the hyperintruder levels

In studies of superdeformed bands, it was always pointed out that the contributions to the total angular momenta I,

TABLE II. Contribution of all occupied intruder orbitals [N,N,0]1/2 to the kinematical moment of inertia $J^{(1)}$ in the nucleus ^{122}Xe. The results are given at constant rotational frequencies $\omega = 0.6, \ldots, 0.9$ MeV for the superdeformed (columns 5 to 8) and hyperdeformed configuration (columns 1 to 4). For a given intruder N, the first line refers to the neutron and the second to the proton. The last four lines give the total $J^{(1)}$ moment brought by the neutron intruders, protons intruders, the sum of all (n and p) intruders, and the total moment of inertia of the nucleus.

Columns	(hd)	(hd)	(hd)	(hd)	(sd)	(sd)	(sd)	(sd)
ω	0.6	0.7	0.8	0.9	0.6	0.7	0.8	0.9
$N = 1$	1.347	1.351	1.357	1.363	1.297	1.288	1.178	1.168
	1.372	1.378	1.337	1.191	1.122	1.118	1.144	1.108
$N = 2$	1.947	1.887	1.908	1.890	2.292	2.260	2.225	2.187
	1.633	1.620	1.605	1.588	2.133	2.009	1.983	1.955
$N = 3$	3.527	3.352	3.305	3.083	3.702	3.612	3.502	3.345
	3.138	3.064	2.985	2.907	3.201	2.923	2.590	1.926
$N = 4$	2.189	1.950	1.771	1.757	5.551	5.378	5.189	4.988
	1.960	1.798	1.664	1.568	5.067	4.826	4.517	4.606
$N = 5$	4.351	4.083	3.766	2.920	7.475	7.248	6.970	6.081
	3.663	3.434	3.180	2.921	7.284	6.996	6.680	5.460
$N = 6$	5.887	4.514	3.564	3.991	9.013	8.907	8.248	7.253
	5.082	5.035	4.611	4.094	8.065	8.408	7.645	6.698
$N = 7$	8.195	7.561	5.004	6.312	6.895	4.946	5.344	5.354
	7.883	7.271	5.753	4.463	–	–	–	–
Total (n)	27.44	24.60	20.68	21.32	36.23	33.64	32.66	30.38
Total (p)	24.73	23.60	21.13	18.73	26.87	26.28	24.56	21.75
Total Int.	52.17	48.20	41.81	40.05	63.10	59.92	57.22	52.13
Total	107.8	107.0	106.4	105.9	83.3	82.4	82.7	81.0

hence, to the total kinematical moment of inertia, $J^{(1)} = I/\omega$, from the intruder orbitals are very significant. We give in Table II the kinematical moment of inertia $J_\nu^{(1)}$ of the states ν corresponding to all the (occupied) intruder orbitals in the case of ^{122}Xe. To simplify comparison we define the corresponding contributions as

$$J_\nu^{(1)} = -\left[\frac{de_\nu^\omega}{d\omega} + \frac{d\bar{e}_\nu^\omega}{d\omega}\right], \tag{14}$$

where e_ν^ω is the single-particle Routhian at frequency ω and $\bar{e}_\nu^\omega$ its signature partner. In axially deformed nuclei, the intruder orbitals are defined at null rotational frequency by $\ell_z = 0$. These are the orbitals that are the most aligned with the collective rotation axis. Their Nilsson labels, $[N, n_z, \ell_z]K$, are of the type $[N, N, 0]1/2$ with N referring to the oscillator shell number. As the rotational frequency increases neither ℓ_z nor K remains a good quantum number. The nucleonic wave functions are of course expanded onto the harmonic-oscillator basis, and the label of the basis function with the largest weight is conventionally assigned to the physical state. In this nucleus, the SD configuration (columns 5 to 8) is characterized by $\beta_2 = 0.70$, $\beta_4 = 0.10$, and $\beta_6 = -0.01$ and the HD one (columns 1 to 4) by $\beta_2 = 1.10$, $\beta_4 = 0.17$, $\beta_6 = -0.03$, and $\beta_8 = -0.02$.

From reading Table II, we notice that the contribution to the total $J^{(1)}$ from the intruder orbitals can amount to up to 75% of the total in the superdeformed case at $\omega = 0.6$ MeV. On average, it typically contributes to about 70% of the total $J^{(1)}$. By comparison, in the hyperdeformed case this same contribution is less important, although the $N = 7$ proton orbital is now additionally occupied. In the range of rotational frequency considered here (which corresponds roughly to the range of spin $I \sim 50$–$73\hbar$ for the superdeformed case and $I \sim 65$–$95\hbar$ for the hyperdeformed case), the intruder orbitals thus contribute for up to 46% at $\omega = 0.6$ MeV and about 40% on average. Consequently, if one may claim rightly that the intruder orbitals play a critical role in building up the kinematical moment of inertia in the superdeformed case, this affirmation must certainly be nuanced for hyperdeformed nuclei.

In fact, the origin of the very large moments of inertia in hyperdeformed nuclei is to be found in another mechanism. In Table III we give for the same nucleus and the same super- and hyperdeformed configuration the number of single-particle down-sloping and up-sloping orbitals, the contribution to the total $J^{(1)}$ of both classes of orbitals, and the total $J^{(1)}$ itself. As deformation is increasing, the ratio down-sloping/up-sloping orbitals (in the vacuum configuration) is decreasing. This is a natural consequence of the pseudo-SU(3) multiplet distribution in the near-constant depth potential generated by the nuclear mean-field Hamiltonian. Because the contribution of the level ν to the total $J^{(1)}$ is given by Eq. (14), the more down-sloping orbitals are occupied in a given configuration, the more numerous are the positive contributions to the total

TABLE III. Comparison of the moments of inertia in the SD and HD geometries for ^{122}Xe. For several rotational frequencies ω, the table reports, in each geometry, the number of down-sloping $N(-)$ and up-sloping $N(+)$ orbitals, the total kinematical moment of inertia $J^{(1)}(-)$ (respectively $J^{(1)}(+)$) of the down-sloping (respectively up-sloping) orbitals, and the total $J^{(1)}$ moment of the given geometry.

^{122}Xe	ω	$N(-)$	$N(+)$	$J^{(1)}(-)$	$J^{(1)}(+)$	$J^{(1)}_{\text{tot}}$
SD	0.6	53	69	−16.1	99.4	83.3
SD	0.7	49	73	−14.2	98.6	82.4
SD	0.8	44	78	−12.6	95.3	82.7
SD	0.9	43	79	−12.1	93.1	81.0
HD	0.6	24	98	−5.6	113.4	107.8
HD	0.7	21	101	−3.5	110.5	107.0
HD	0.8	13	109	−2.0	108.4	106.4
HD	0.9	12	110	−1.7	107.6	105.9

$J^{(1)}$. Given the fact that the intruder orbitals are by definition all down-sloping as a function of deformation, the comparison of the results in Tables II and III provides a qualitative understanding of the microscopic basis for the increase in the moments of inertia as a function of the deformation and the differentiated roles of the intruder orbitals in the case of SD and HD nuclei.

The kinematical and dynamical moments are related by the expression

$$J^{(2)}(\omega) = J^{(1)}(\omega) + \omega \frac{dJ^{(1)}(\omega)}{d\omega}. \tag{15}$$

From the observation that the curves $J^{(1)}(\omega)$ are very flat with respect to the rotational frequency ω (see Fig. 10), we obtain the approximate equality

$$J^{(2)}(\omega) \sim J^{(1)}(\omega) \sim J_{\text{rig}}. \tag{16}$$

This relation is also valid for the hyperdeformed configuration of all the nuclei studied in this section. In fact, such a feature was already stressed in the framework of superdeformation. It was interpreted as a consequence of the fact that no strongly aligned down-sloping orbitals cross the Fermi level within broad ranges of the rotational frequencies considered [27]. There are thus certain similarities between the behavior of the SD and HD nuclei at high spins. Indeed, both geometries lead to very collective rotation. In the SD case, this is a well-known feature of many superdeformed bands, e.g., in the mass $A \sim 150$ as seen in experiment. However, the contributions from the intruder orbitals to the total angular momentum (and to the total kinematical moment of inertia) are quite different (see Table II): the total of these contributions in the HD bands is, relatively, much lower than in the SD bands. As a matter of fact, it does not seem that a particular global property of the HD case could be attributed to the hyperintruders alone, although systematic trends are clear from the Tables II and III.

V. HYPERDEFORMATION IN SELECTED REGIONS OF THE NUCLEAR CHART

The hyperdeformation phenomenon is expected in various nuclear mass ranges, the range of $A \sim 120$ being characterized by the highest fission barriers as compared to other ones—and thus probably the most favorable. On the other hand it is not excluded that shell effects stabilizing the hyperdeformation at low temperatures will be stronger in some other mass ranges. This problem is largely open; below we focus on a few aspects of it.

A. Rare-earth and heavy nuclei

In Refs. [1] and [6], it was conjectured that hyperdeformed minima can also been found in the rare-earth region. Total Routhian surfaces calculated in this region presented indeed some stable minima at very large deformation. However, a closer inspection of Figs. 1 and 2 reveals that the Jacobi minimum is very shallow as a function of deformation and tends to disappear relatively rapidly with decreasing spin. Although calculations performed at $T = 0$ such as those in Refs. [1] and [6] may exhibit a hyperdeformed minimum, the role of temperature in this region is likely to be decisive for the *population* of the hyperdeformed configurations through the (HI,xn) reactions.

Figure 12 shows the total free energy as a function of the axial quadrupole deformation in ^{152}Dy calculated using the same techniques as those used for Figs. 4 and 5. The excitation energy is fixed at $E^* = 60$ MeV, which corresponds roughly to a temperature of $T \sim 1.0$ MeV. As expected the shell effects are significantly smeared out, which manifests itself by the disappearance of the normal-deformed minimum for $I > 65\hbar$ and the domination of the superdeformed minimum at $\beta_2 \sim 0.6$.

There appears to be a minimum at $I \sim 80\hbar$ at $\beta_2 \sim 0.9$ that may correspond to hyperdeformation, as illustrated in Ref. [6] (observe that the scale in the ordinate axis is very

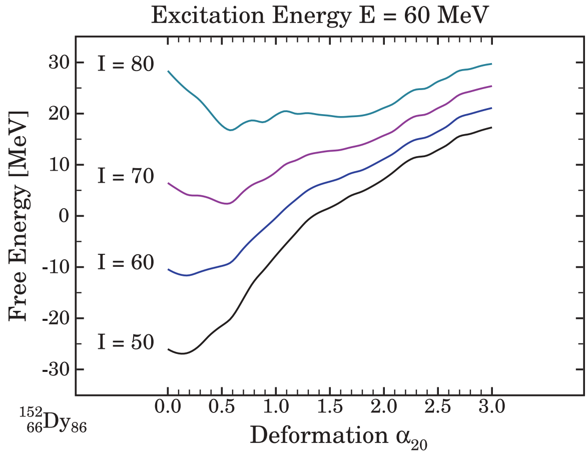

FIG. 12. (Color online) Total free energy curves in ^{152}Dy as a function of the elongation, for an excitation energy of $E^* = 60$ MeV. The details of the calculations are the same as in the similar Figss. 4 and 5.

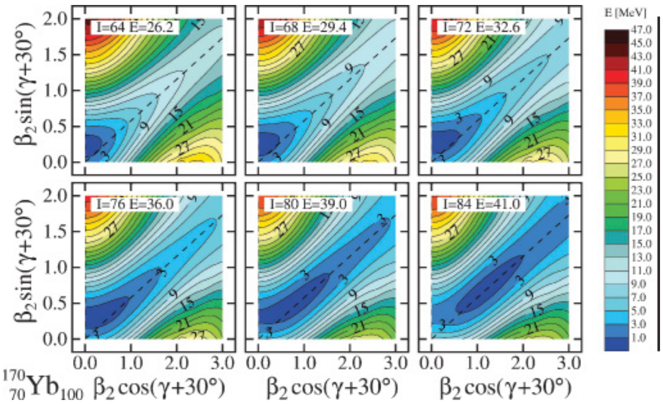

FIG. 13. (Color online) Total energy surfaces in ^{170}Yb in the liquid drop regime (no shell correction, high temperature limit). The figure is similar to Fig. 3, using the techniques of calculations presented in Sec. II.

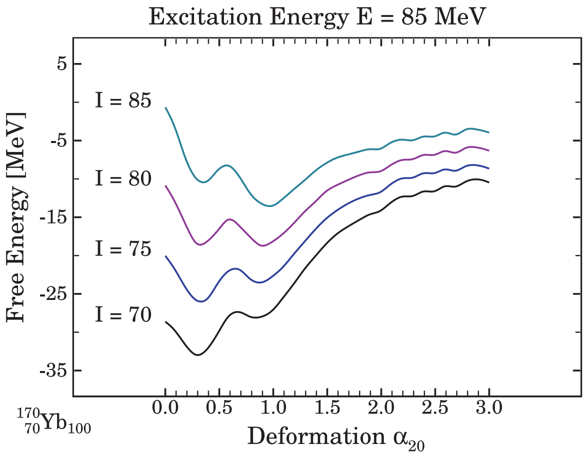

FIG. 14. (Color online) Total free energy of the ^{170}Yb nucleus as function of the elongation $\alpha_{20} \equiv \beta_2$ at a fixed excitation energy $E^* = 85$ MeV (corresponding to maximum temperatures of the order of 1.5 MeV). Similar as Fig. 4.

extended and the minimum mentioned is a few MeV deep). Similarly, the possible existence of a *megadeformed* minimum at this spin with elongations of the order of $\beta_2 \sim 1.5$ cannot be entirely dismissed and is discussed in Ref. [2]. However, the superdeformed minimum at $\beta_2 = 0.6$ appears to be significantly deeper and lower than the aforementioned ones and it is thus likely that it will be populated with the highest probability.

Consequently, with present-day experimental techniques, it seems that the conjunction of a flat-minimum Jacobi transition (see Figs. 1 and 2) together with the particularly large shell gaps such as $Z = 66$ and $N = 86$ (resisting to some extent to the thermal excitation) leads to the privileged population of the superdeformed band. This does not imply that no hyperdeformed configurations (or even megadeformed ones) exist in this region, but rather that the reaction mechanisms should be sought to populate these states by "avoiding as much as possible" the high-temperature regime.

The rare-earth region is characterized by a *sequence* of superdeformed magic numbers (as a consequence of the pseudo-SU(3) symmetry, see Refs. [5] and [1] and Fig. 2 in Ref. [3]). However, nuclei from the rare-earth region whose numbers of protons and neutrons differ from this sequence may remain potentially interesting candidates. An example of such a nucleus that has drawn continued interest is ^{170}Yb. In Fig. 13, we show the liquid-drop potential energy surface from $I = 64\hbar$ to $I = 84\hbar$. The nature of the Jacobi transition resembles that of ^{152}Dy. The nucleus ^{170}Yb is characterized by a shallow minimum. However, a characteristic that may have important experimental consequences is the fact that the transition occurs at slightly higher spins: it roughly starts at $I = 76\hbar$ and is completed at $I = 82\hbar$. One must bear in mind that calculations such as those in Fig. 13 are valid in the exact limit of the liquid-drop regime, when all shell effects are identically 0. For nuclei like ^{170}Yb, our calculations show that the *total* disappearance of the shell effects corresponds to temperatures of up to $T \sim 2.5$–3.0 MeV. Consequently, full-scale macroscopic-microscopic calculations taking into account the thermal excitations are required to assess whether the HD regime is accessible in this nucleus indeed.

Figure 14 shows the behavior of the total free energy at $E^* = 85$ MeV of excitation energy, corresponding to maximum temperatures of $T \sim 1.5$ MeV. We chose this value of the excitation energy to approach the experimental conditions of the (unsuccessful) search for hyperdeformation in ^{168}Yb published in Ref. [28]. Two minima appear neatly: one with $\beta_2 \sim 0.35$, which corresponds to normal deformation, and the other one with $\beta_2 \sim 1.0$, which corresponds to hyperdeformation.

It is worth noting that in accordance with the pure liquid-drop result illustrated in Fig. 13, where shell effects are identically zero, the fission barrier still amounts to about 10 MeV for this choice of excitation energy at $I = 80\hbar$ (around 7–8 MeV if $\lambda > 8$ multipoles are taken into account). In addition, inspection of Fig. 14 suggests that the well-defined hyperdeformed minimum appears already at $I \sim 70\hbar$. In the nucleus ^{170}Yb, the hyperintruder orbitals come from the $N_{\rm sph} = 7$ shell for the protons and the $N_{\rm sph} = 8$ shell for the neutrons. In the second minimum in Fig. 14, both types of hyperintruder orbitals are occupied.

The nucleus ^{170}Yb thus represents an interesting case. On the one hand, it does possess a hyperdeformed minimum that appears for $I > 70\hbar$ or so and becomes yrast at about $I \sim 80\hbar$. This minimum is separated from the normal-deformed minimum by a large barrier of about 5 MeV, and the fission barrier is of the order of 10 MeV. Moreover, there is no superdeformation at the spins involved, so that the number of competing configurations reduces to two (compared to three in the mass $A \sim 130$). On the other hand, the population of this hyperdeformed minimum is likely to require a very careful experimental setup. Indeed, enough angular momentum must be supplied to the system to reach the Jacobi transition at about $I \sim 80\hbar$ or higher.

It is possible that one of the reasons why the experiment reported in Ref. [28] was not successful was precisely the lack of angular momentum in the daughter nucleus ^{168}Yb. Although the compound nucleus ^{172}Yb was formed at an approximate $L_{\max} = 87\hbar$, the evaporation of four neutrons was probably sufficient to lower substantially the angular momentum by $\sim$ 6 to $8\hbar$. Reaching the hyperdeformed minimum at high temperatures may still be possible by studying the Giant Dipole Resonance (GDR) built on hyperdeformed states in the high-temperature regime.

B. The case of ^{108}Cd

In Ref. [7], evidence was reported of a "very extended quadrupole ellipsoidal shape" in ^{108}Cd for an angular momentum window of $\Delta I = 40$–$60\hbar$. The dynamical moment $J^{(2)}$ deduced from the γ-transition energies was estimated at about $J^{(2)} \sim 51\hbar$ MeV^{-1}. The authors concluded from their results that the reported band corresponded to "one of the most deformed structures ever observed." In Fig. 9, which shows the single-particle Routhians as a function of ω in the HD minimum for the region $A \sim 120$–130, the most prominent proton shell gap corresponds to $Z = 48$, therefore suggesting that Cd isotopes may also be among the best candidates for hyperdeformation. Let us note that for nuclei with $28<Z<50$ and $50<N<82$ like ^{108}Cd, the proton hyperintruders are the $N_{\text{sph}} = 6$ orbitals while the neutron ones are the $N_{\text{sph}} = 7$ orbitals.

Figure 15 shows indeed that there exists a very deformed minimum at an elongation $\beta_2 \sim 0.9$–1.0. Nevertheless, at high excitation energy (high temperatures) this minimum becomes yrast only at a spin of about $I \sim 60\hbar$, corresponding to the beginning of the Jacobi transition in this nucleus. This value of the angular momentum is in the upper limit of the spin window reported in Ref. [7], but the results shown in Fig. 15 suggest that hyperdeformed states could *not* be populated at lower spins.

Calculations performed at lower excitation energy such as in Fig. 16 suggest that, between $I = 40\hbar$ and $I = 60\hbar$, there exists a competition among an ND minimum with $\beta_2 \sim 0.4$, an SD one with $\beta_2 \sim 0.7$, and an HD one with $\beta_2 \sim 0.9$. At an angular momentum $I \sim 60\hbar$, all three minima have nearly the same energy, although they are separated from each other by significant barriers.

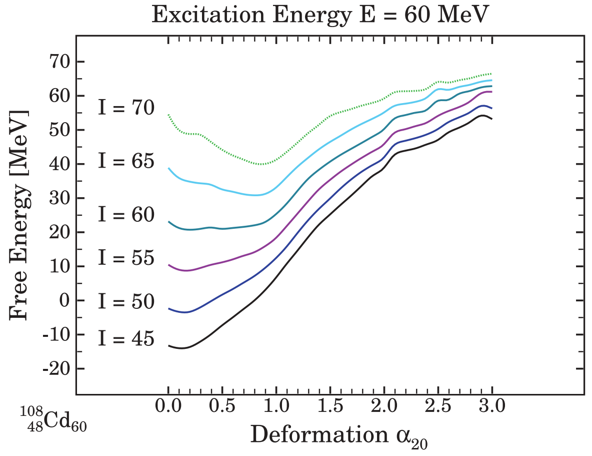

FIG. 15. (Color online) Total free energy of ^{108}Cd as a function of the quadrupole elongation $\beta_2 \equiv \alpha_{20}$ for an excitation energy of $E^* = 60$ MeV, characteristic of a high-temperature regime. Higher-order multipoles β_4, β_6, and β_8 are obtained from the minimization of the total free Routhian.

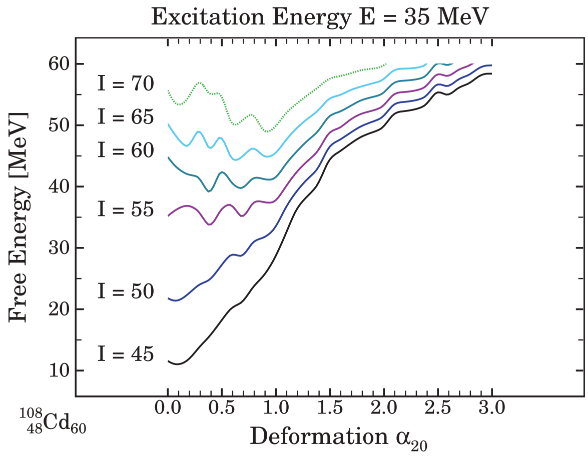

FIG. 16. (Color online) Total free energy of ^{108}Cd as a function of the quadrupole elongation $\beta_2 \equiv \alpha_{20}$ for an excitation energy of $E^* = 35$ MeV, characteristic of low temperatures.

We applied to this nucleus the techniques presented in the previous sections to compute the dynamical moments in various minima. We considered as before different particle-hole excitations built on the vacuum configuration. Figure 17 shows the dynamical moments for the ten lowest particle-hole excitations in the superdeformed minimum (characterized by $\beta_2 = 0.7$). There appear two families of bands: The first one is characterized by a relatively constant moment of inertia around $J^{(2)} \sim 55\hbar$ MeV^{-1}. This family corresponds to one-particle one-hole excitations such that superintruder [660]1/2 (Fig. 19) is unoccupied and one of the levels above the gap $N = 60$ is occupied.

In the second family, where the superintruder orbital [660]1/2 remains occupied, the dynamical moment is slightly more sensitive to the angular momentum and varies from $J^{(2)} \sim 62\hbar$ MeV^{-1} to $J^{(2)} \sim 55\hbar$ MeV^{-1}. These values appear very close to the results of Ref. [7].

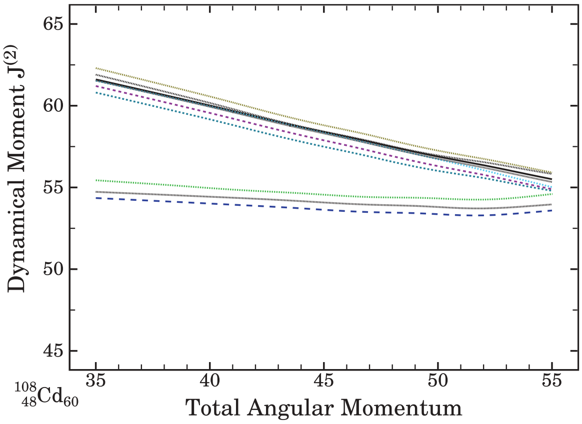

FIG. 17. (Color online) Dynamical moments in ^{108}Cd at $T = 0$ for the ten lowest particle-hole excitations built on the vacuum configuration as a function of the angular momentum. The elongation is fixed at $\beta_2 = 0.7$.

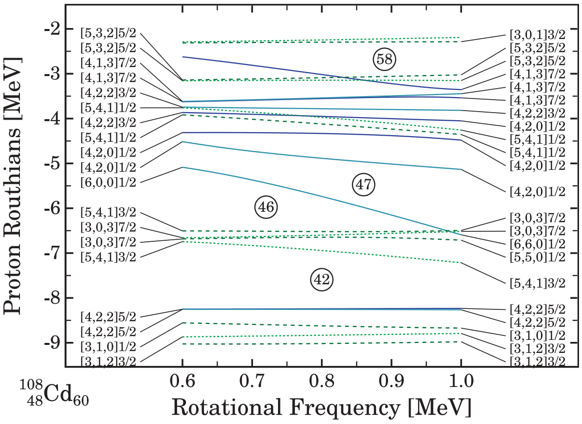

FIG. 18. (Color online) Proton single-particle Routhians at $T = 0$ in ^{108}Cd as a function of the rotational frequency. The deformations correspond to the “superdeformed” minimum with $\beta_2 = 0.7$. The lowest hyperintruder is the [660]1/2 orbital (label at approximately -6.5 MeV in the right-hand side of the figure) and is occupied for the whole range of rotational frequency considered, which corresponds roughly to the experimental range of spin $40\hbar \leqslant I \leqslant 60\hbar$.

The microscopic structure of what we called a “superdeformed” minimum is illustrated in Figs. 18 and 19. The figures show the single-particle Routhians for the protons (upper frame) and the neutrons (lower frame) as a function of the rotational frequency ω. The range of the latter correspond approximately to the range of angular momentum $40\hbar < I < 60\hbar$. Both superintruder orbitals are occupied. Additionally, in the case of the protons the hyperintruder [660]1/2 level is also occupied, but the corresponding neutron hyperintruder level is not. Consequently, the structure of this minimum is a kind of hybrid between hyper- and superdeformed. A detailed analysis of all reported excited bands in ^{108}Cd within the framework of the cranked relativistic mean-field led essentially to the same conclusions [8].

We also calculated the dynamical moments in the third minimum at $\beta_2 = 1.0$. The results are reported in Fig. 20. The dynamical moments are larger than the values reported in Ref. [7] by 50%. Moreover, we see clearly that even though the precise value of the moment of inertia may vary from one particle-hole configuration to the other, these differences do not exceed 5%. Finally, for the value of the elongation $\beta_2 = 1.0$, both the proton and neutron hyperintruder orbitals are occupied (see Figs. 18 and 21).

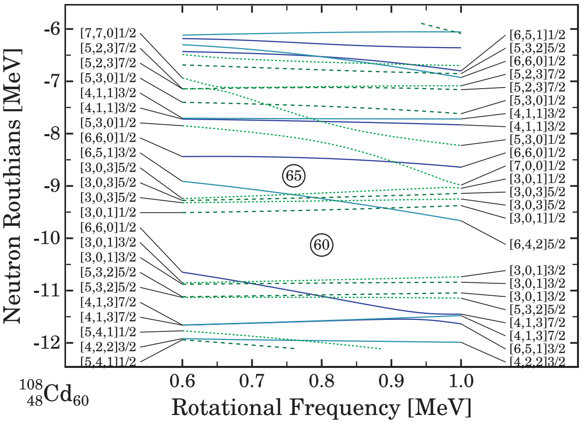

FIG. 19. (Color online) Same as Fig. 18 but for the neutrons. The lowest hyperintruder is the [770]1/2 orbital (first from the top left-hand side of the figure) and is not occupied for $N = 60$.

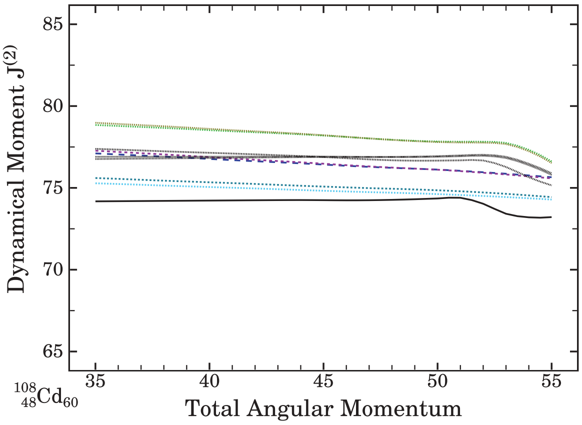

FIG. 20. (Color online) Dynamical moments in ^{108}Cd at $T = 0$ for the ten lowest particle-hole excitations built on the vacuum configuration as a function of the angular momentum. The elongation is fixed at $\beta_2 = 1.0$ and corresponds to the “true” HD minimum.

Nontheless, this nucleus may still remain one of the most favorable candidates for observing *discrete* transitions in the hyperdeformed well. Indeed, it cumulates a number of favorable criteria. First, there is a neat hyperdeformed minimum that becomes yrast at a spin of $I \sim 60\hbar$. Second, the fission barrier appears to be particularly large. This suggests that the HD minimum could survive fission for a significant range of angular momentum. Nuclei of the mass $A \sim 100$ are known to be among those that can be populated at the highest spins. Finally, the clear difference in the dynamical moments between the superdeformed and the true hyperdeformed configuration should lead to the unambiguous identification of the underlying structure of the bands.

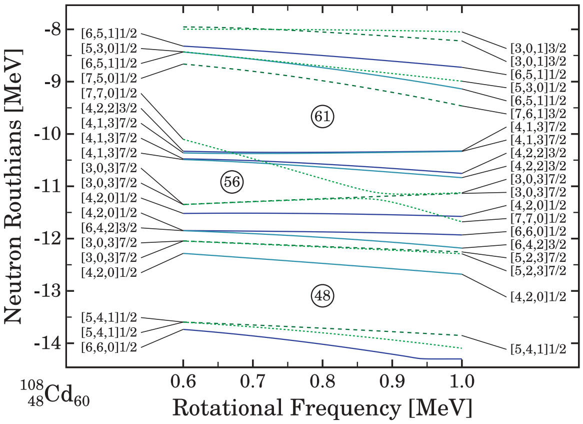

FIG. 21. (Color online) Same as Fig. 19 but for the deformations corresponding to the “true” hyperdeformed minimum with $\beta_2 = 1.0$. The lowest hyperintruder is still the [770]1/2 orbital which is now occupied for $\omega \geqslant 0.65$ MeV.

VI. SUMMARY AND CONCLUSIONS

Realistic mean-field calculations based on the macroscopic-microscopic method spanning a large deformation space and including the standard description of thermal effects suggest the existence of hyperdeformed configurations in the mass $A \sim 130$ Xe-Ba isotopes. These configurations are characterized by an axial elongation of $\beta_2 \sim 1.1$ on the average corresponding to the axis ratio "long:short" of the order of 2.5:1. They become yrast at spins $I > 70\hbar$ and completely disappear already at $I \sim 60\hbar$. In the isotopes considered in this mass region the population of hyperdeformed states is in competition with that of the normal-deformed (first) and superdeformed (second) minimum and with the fission process; this competition makes it impossible for long hyperdeformed bands to build up, because the corresponding nuclei either fission or decay to one of the states with the smaller deformations.

Both the kinematical and dynamical moments in the hyperconfiguration are nearly straight lines as a function of the angular momentum. Moreover, because the underlying single-particle Routhians are very regular and nearly linear functions of the rotational frequency, the corresponding particle-hole configurations lead to numerous bands with very close moments of inertia. The average dynamical moments in the hyperdeformed configurations thus lie around $J^{(2)} \sim 100 \pm 10\hbar\ \text{MeV}^{-1}$, in the considered $A \sim 130$ Xe-Ba region, depending slightly on the nucleus under consideration. In the case of ^{124}Xe, ^{125}Cs, and ^{118}Te, the calculated values fall within the error bars of the experimental values. When calculated in the superdeformed configuration, the theoretical moments of inertia are found to be lower than the experimental values by 20–30%.

It is emphasized that the large moments of inertia should not be attributed solely to the occupation of the so-called hyperintruder and/or superintruder orbitals. To the contrary, the contribution of all the intruder orbitals to the total moments of inertia is found to be significantly lower in the hyperdeformed minima as compared to the superdeformed ones. Instead, we suggest that the origin of these large moments must be found in the ratio down-sloping/up-sloping (with respect to the rotational frequency ω) orbitals in a given configuration.

In other mass regions, it is emphasized that heavy nuclei present the disadvantage of having much smaller fission barriers. This has important consequences because hyperdeformation should be seen as intrinsically the highest-spin-limit phenomenon, triggered by the Jacobi shape transition. Consequently, even though the prediction of the existence of the hyperdeformed configurations in several cases (like, e.g., ^{152}Dy and ^{170}Yb) is confirmed by our calculations, the main difficulties in observing such states, and *a fortiori* discrete transitions, would be of an experimental nature. A compromise must be found so that the transferred angular momentum matches the relatively narrow spin window, sometimes as narrow as $\Delta I = (4\text{–}6)\hbar$, to reach the Jacobi regime without leading to fission.

Conversely, although the results published for ^{108}Cd cannot be interpreted as the signature of a "pure" hyperdeformed configuration, this nucleus remains nevertheless a very promising candidate for the design of future experiments. Perhaps gating on the SD band could purify the condition for finding hyperdeformed structures at even higher spins.

Several conditions can thus be underlined to successfully observe discrete transitions associated with the hyperdeformed minimum. First, a well-pronounced Jacobi shape transition is required in the mother nucleus, which (like in the mass $A \sim 130$ region) must be characterized by a well-deformed minimum at very high spin. This is necessary to have a sufficiently long window of angular momentum where the hyperdeformed state could decay. In addition, the presence of long superdeformed bands in the daughter nuclei will hinder hyperdeformation as it most likely signals the presence of strong shell effects associated with superdeformed shell gaps. As the nucleus cools down, these superdeformed bands are likely to attract a major part of the feeding.

ACKNOWLEDGMENTS

This work is partially supported by the exchange programme between IN2P3 (France) and Polish Nuclear Physics Laboratories and by The Danish Science Foundation.

---

[1] J. Dudek, T. Werner, and L. L. Riedinger, Phys. Lett. **B211**, 252 (1988).
[2] J. Dudek, K. Pomorski, N. Schunck, and N. Dubray, Eur. Phys. J. A **20**, 15 (2003).
[3] J. Dudek, N. Schunck, and N. Dubray,Acta Phys. Pol. B **36**, 975 (2005).
[4] J. Dudek and W. Nazarewicz, Phys. Rev. C **31**, 298 (1985).
[5] J. Dudek, W. Nazarewicz, Z. Szymanski, and G. A. Leander, Phys. Rev. Lett. **59**, 1405 (1987).
[6] T. R. Werner and J. Dudek, At. Data Nucl. Data Tables **50**, 179 (1995); T. R. Werner and J. Dudek, At. Data Nucl. Data Tables **59**, 1 (1995).
[7] R. M. Clark *et al.*, Phys. Rev. Lett. **87**, 202502 (2001).
[8] A. V. Afanasjev and S. Frauendorf, Phys. Rev. C **72**, 031301(R) (2005).
[9] B. Herskind *et al.*, Acta Phys. Pol. B **34**, 2467 (2003).
[10] B. Herskind *et al.*, AIP Conf. Proc. **701**, 303 (2004).
[11] H. Hübel, Acta Phys. Pol. B **36**, 1015 (2005).
[12] B. M. Nyako *et al.*, Acta Phys. Pol. B **36**, 1033 (2005).
[13] C. Rønn Hansen *et al.*, AIP Conf. Proc. **764**, 46 (2005).
[14] B. Herskind *et al.*, Phys. Scr. T **125**, 1 (2006).
[15] Robert Beringer and W. J. Knox, Phys. Rev. **121**, 1195 (1961); S. Cohen, F. Plasil, and W. J. Swiatecki, Ann. Phys. (NY) **82**, 557 (1974); Arnold J. Sierk, Phys. Rev. C **33**, 2039 (1986).
[16] D. Ward *et al.*, Phys. Rev. C **66**, 24317 (2002).
[17] A. Maj *et al.*, Nucl. Phys. **A731**, 319 (2004).
[18] A. Bohr and B. R. Mottelson, *Nuclear Structure* (Benjamin, Addison-Wesley, 1969), Vol. II.
[19] K. Pomorski and J. Dudek, Phys. Rev. C **67**, 044316 (2003).

[20] T. Lauritsen *et al*., Phys. Rev. Lett. **88**, 042501 (2002).
[21] V. M. Strutinsky, Nucl. Phys. **A95**, 420 (1967); V. M. Strutinsky, Nucl. Phys. **A122**, 1 (1968).
[22] J. Dudek, Z. Szymanski, and T. R. Werner, Phys. Rev. C **23**, 920 (1980).
[23] J. Dudek, in *Proceedings of the International Winter Meeting on Nuclear Physics, Bormio, Italy, 1987 (Ricerca Scientifica ed Educazione Permanente, Supplemento N. 56*, edited by I. Iori).
[24] J. Dudek, B. Herskind, W. Nazarewicz, Z. Szymanski, and T. R. Werner, Phys. Rev. C **38**, 940 (1988).
[25] T. Bengtsson, Nucl. Phys. **A496**, 56 (1989); **A512**, 124 (1990).
[26] W. Nazarewicz, in *Contemporary Topics in Nuclear Structure Physics*, edited by R. F. Casten, A. Frank, M. Moshinsky, and S. Pittel (World Scientific, Singapore, 1989), p. 467.
[27] T. Bengtsson and I. Ragnarsson, Nucl. Phys. **A436**, 1 (1985).
[28] J. N. Wilson *et al*., Phys. Rev. C **56**, 2502 (1997).